Plasma electrolytic oxidation of Ti - W surface alloys synthetized by PVD-LEHCEB

Plasma electrolytic oxidation of Ti - W surface alloys synthetized by PVD-LEHCEB

F Morini[1,3], S Franz[1], A Vicenzo[1] and M Bestetti[1,2]

[1] Politecnico di Milano, Department of Chemistry, Materials and Chemical Engineering "G. Natta", Via Luigi Mancinelli 7, Milano, 20131, Italy
[2] Tomsk Polytechnic University, The Weinberg Research Center, 30 Lenin Ave., Tomsk, 634050, Russia

[3] E-mail: federico.morini@polimi.it

Abstract. An innovative approach exploiting PVD-coupled Low-Energy High-Current Electron Beam (LEHCEB) and Plasma Electrolytic Oxidation (PEO) techniques were investigated to obtain photoactive TiO_2-WO_3 mixed films. Ti-W surface alloys containing 14 at.% W were synthetized by PVD deposition of 185 nm thick W films onto Ti substrates, followed by LEHCEB alloying at 30 kV for 50 pulses. The obtained Ti-W surface alloys were treated by PEO in 1.5 M H_2SO_4 at constant cell voltage ranging from 100 to 200 V. The resulting mixed oxide films were investigated by XRD, SEM and EDS analysis. Photoelectrochemical properties were determined by linear sweep voltammetry in dark and under UV-C and UV-VIS irradiation.

1. Introduction

Alloying Ti with refractory metals is a useful route to enhance its properties [1]. Ti-W alloys raised attention because W can induce higher hardness and wear resistance due to the possible formation of several metastable phases [2, 3] Additionally, W alloying results in higher corrosion resistance and melting point, and low atomic diffusivity, which are fundamental properties for different applications [4]. Producing surface thin films allows to maintain Ti bulk properties, at the same time enhancing the features of the outermost micrometric layer of the material. Low-Energy High-Current Electron Beam (LEHCEB) is one of the promising ways to produce surface alloys with graded composition [5]. Indeed, LEHCEB has been proposed for surface modification and surface alloying, including grain refinement and the formation of metastable phases with enhanced mechanical and corrosion resistance properties compared to the substrate materials [6, 7].

Ti-W alloys attracted attention also for the possibility to produce mixed oxide systems for photocatalytic applications. TiO_2 is an extensively studied photocatalyst having a relatively large band-gap (~ 3.2 eV anatase and ~ 3.02 eV rutile) and has been widely applied in waste-water treatment and water splitting [8, 9]. WO_3 as well has been investigated as photocatalyst due to its small band gap (~ 2.8 eV) and higher light adsorption in the visible range [10, 11]. Mixtures of WO_3 and TiO_2 has been proved to outperform the individual oxides both in terms of photocatalytic activity [12-14]. Mixed TiO_2-WO_3 films were obtained by reactive magnetron co-sputtering [15], thermal oxidation [12], electrospinning [13] and anodization of Ti in electrolytes containing W precursors [16]. An attractive alternative is plasma electrolytic oxidation (PEO) of Ti. This process promotes the

instantaneous formation of crystalline oxides [17-20] and has attracted attention as a promising route to produce large area photoelectrodes for water treatment and solar-assisted hydrogen production [21-24]. Despite these promising features, PEO has been hardly investigated for the synthesis of mixed TiO_2 and WO_3 films [25, 26].

In this work mixed TiO_2 and WO_3 films were obtained by PVD-coupled LEHCEB followed by PEO. Crystallographic, morphological and photoactivity of alloys and oxides were investigated.

2. Materials and methods

2.1. Sample preparation

Commercially pure (c.p.) Ti ($O \leq 0.08\%$, $C \leq 0.08$ and $Fe < 0.07$) was used as substrate material. Coupons (3×7×0.1 cm) were degreased in a 50/50 vol solution of acetone and ethanol and chemically etched in an aqueous solution of 2 M HF and 1.44 M HNO_3 for 2 min, then rinsed in deionized water and dried in air. RITM-SP facility (Microsplav OOO, Tomsk, Russia) was used for LEHCEB pretreatment and alloy synthesis. All samples were firstly pretreated with LEHCEB at 25 kV and 10 pulses to smoothen the surface and remove contaminants from the surface. After the pretreatment, a 185 nm thick W layer was deposited on the Ti substrate by PVD magnetron sputtering. A W (99.95%) target of 75 mm in diameter was used and a constant current (1.5 A and 380 V) was applied for 5 min. The deposition was followed by LEHCEB alloying treatment at 30 kV and 50 pulses. PEO of the Ti-W surface alloys was carried out in 1.5 M H_2SO_4 at 0°C for 5 min at constant cell voltage (from 100 to 200 V). The electrolyte temperature was controlled by means of a cryostat and an insulated jacketed cell. The cathode was a c.p. Ti grid. The anodized area during PEO was 2 cm^2. For comparison, PEO was also carried out on c.p. Ti samples. Table 1 reports the list of PEO treatments done on different samples.

Table 1. Samples obtained by PEO of c.p. Ti and Ti - W surface alloys.

Sample	PEO voltage (V)
Ti_1; TiW_1	100
Ti_2; TiW_2	120
Ti_3; TiW_3	140
Ti_4; TiW_4	160
Ti_5; TiW_5	180
Ti_6; TiW_6	200

2.2. Sample Characterization

Crystal phase composition was assessed by X-Ray diffraction (XRD) using an EMPYREAN PW1830 diffractometer (PANalytical Ltd.) in grazing incidence configuration (1°, Cu Kα1, λ = 0.15406 nm). Identified peaks were fitted and deconvoluted by Pearson VII fitting function (Origin Pro 2018). Surface morphology and elemental maps were determined by Scanning Electron Microscopy (SEM, ZEISS EVO50VP, Carl Zeiss Jena GmbH) and Energy-Dispersive X-ray Spectroscopy (EDS) (Bruker Quantax 200 6/30 spectrometer, Bruker Corp.), respectively. Linear sweep voltammetry (LSV) was done in a 4 mM KCl aqueous solution in a three-electrode electrochemical cell by using an AMEL 2549 potentiostat (AMEL S.r.l.). Saturated calomel electrode (SCE) was used as reference electrode and a Pt foil as counter electrode. The exposed area for photoelectrochemical measurements was 1 cm^2. LSV was carried out in dark and under UV-C and VIS irradiation (Helios Italquartz S.r.l. and Hamamatsu Photonics K.K., respectively).

3. Results and discussion

3.1. Characterization of Ti-W alloys

The XRD patterns of the sample obtained by PVD-LEHCEB treatment show the presence of Ti-W alloys (figure 1). In particular, in addition to the reflections at $2\theta \approx 35.10°$, 38.39° and 40.16° corresponding to the *hcp* structure of the Ti substrate, peaks at 39.19°, 57.08° and 71.21° were observed, which can be attributed to Ti-W *bcc* β alloys. Based the least-mean square method, a lattice constant of 3.241 Å and a W content of around 14 at.% were calculated.

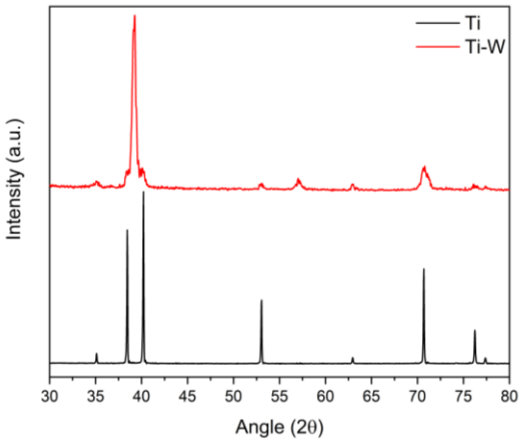

Figure 1. XRD patterns of etched Ti substrate and Ti - W surface alloys.

3.2. Plasma electrolytic oxidation of Ti - W alloys

Figure 2 shows the XRD patterns of the samples after PEO at different cell voltages. A mixture of TiO_2 and WO_3 was observed. The presence of a monoclinic WO_3 phase can be inferred on the basis of the peaks occurring at 35.10° and 40.30° and corresponding to the (220) and (103) reflection planes, respectively. The WO_3 reflections are more intense at lower PEO voltages. According to literature [17], by tuning the cell voltage the anatase-to-rutile relative content was modified. At low voltage (100-120 V), TiO_2 consisted in pure anatase ($2\theta \approx 25.20°$). By increasing the cell voltage, a mixture of anatase and rutile (140 V) and pure rutile (160 - 180 - 200 V) was obtained.

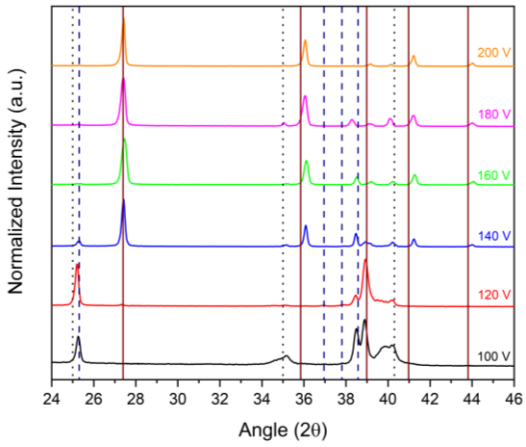

Figure 2. XRD spectra of TiO_2-WO_3 films obtained by PEO in H_2SO_4 solution at different cell voltages. Solid lines represent rutile, dashed lines anatase phase and dot lines WO_3.

The anatase and rutile reflections were shifted with respect to the literature values, indicating a distortion of the TiO_2 lattice. This lattice distortion occurred both along the *a* and the *c* directions (table 2) and overall corresponded to an increase of the unit cell volume. Compared to pure TiO_2 films obtained in the same operating conditions, a stabilization of the rutile phase was observed. Indeed, in

TiO_2-WO_3 films rutile is the prevailing phase at cell voltages (140-160 V) where usually almost equimolar mixtures of anatase and rutile are obtained [18]. This could have a beneficial effect in view of applications in solar assisted energy conversion and catalysis, given the lower energy band-gap of rutile with respect to anatase.

Table 2. Lattice parameter and cell volume of anatase and rutile in TiO_2-WO_3 films. (Anatase: a = 3.785 Å, c = 9.514 Å, V = 136.300 Å^3; Rutile: a = 4.653 Å, c = 2.969 Å, V = 64.280 Å^3).

Sample	Anatase			Rutile		
	a (Å)	c (Å)	V (Å^3)	a (Å)	c (Å)	V (Å^3)
TiW_1	3.794	9.499	136.767	4.628	2.969	63.596
TiW_2	3.806	9.491	137.459	4.618	2.969	63.322
TiW_3	3.794	9.485	136.532	4.607	2.954	62.691
TiW_4	3.791	9.515	136.750	4.592	2.956	62.339
TiW_5	3.718	9.862	140.756	4.600	2.961	62.663
TiW_6	-	-	-	4.598	2.960	62.579

According to SEM micrographs (figure 3), the surface morphology was porous and sponge-like. At 120 V the surface morphology strongly resembled that of pure TiO_2 [18]. On the other hand, at higher cell voltages the surface morphology differentiated from that of pure TiO_2 films, showing coarser and less homogeneous features. Correspondingly, EDS analysis and the related elemental maps demonstrate an higher content (from 3.2 at.% at 120 V to 0.3 at.% at 200 V) and more homogenous distribution of W at lower cell voltages (table 3). This is in agreement with XRD spectra, where the most intense WO_3 peaks were observed in samples synthetized at lower cell voltages.

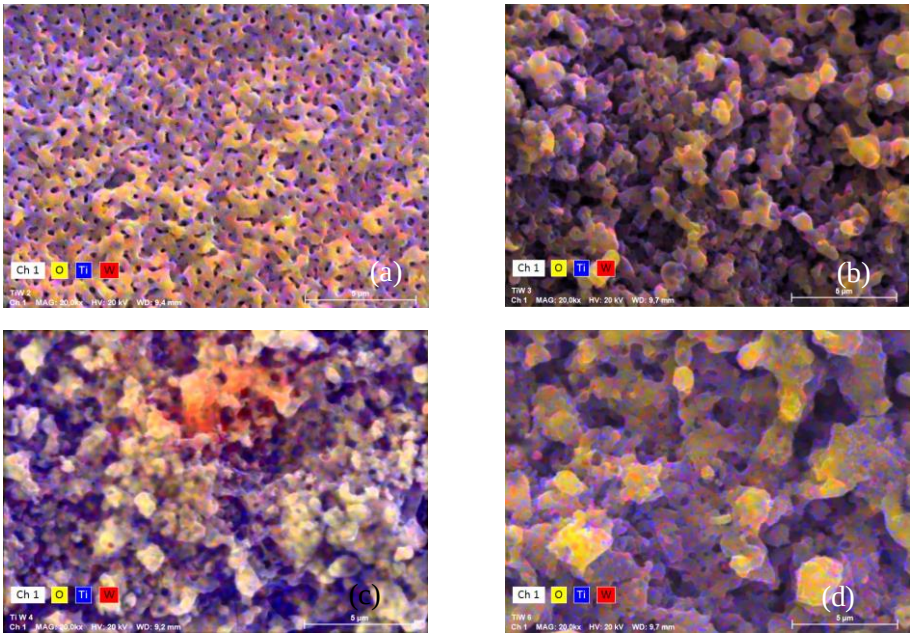

Figure 3. SEM micrographs and corresponding elemental maps of Ti-W oxide obtained at 120 (a), 140 (b), 160 (c) and 200 V (d).

Table 3. EDS W content evaluated in Ti-W samples.

Sample	TiW_1	TiW_2	TiW_3	TiW_4	TiW_5	TiW_6
W content (at.%)	3.5	3.2	1.4	0.6	0.4	0.3

3.3. Photoactivity of oxides

In figure 4, the photocurrent of pure TiO_2 films (figure 4 (a)) and TiO_2-WO_3 films (figure 4 (b)) are showed.

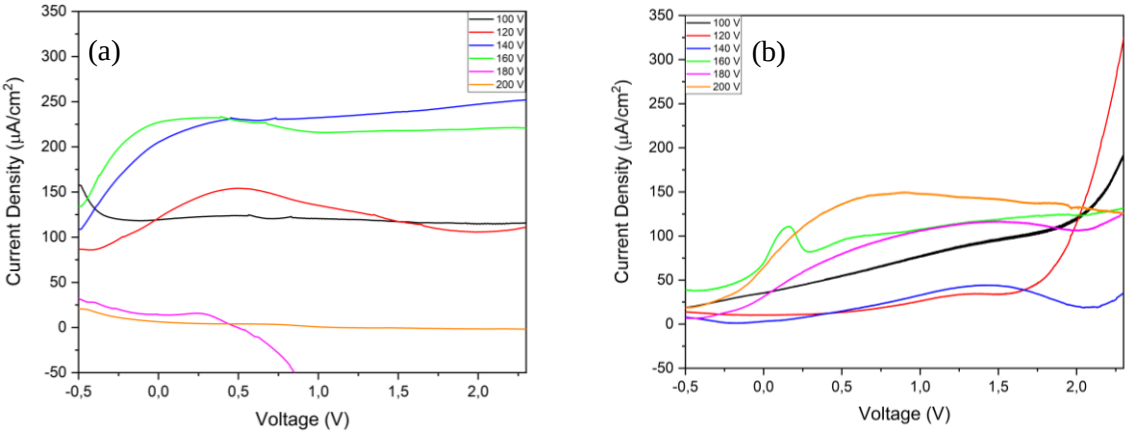

Figure 4. Photocurrent density of TiO_2 (a) and Ti-W oxide (b) samples under UV-C irradiation.

Table 4. Photocurrent values of TiO_2 and Ti-W oxide samples during LSV at 0.5 and 1.5 V under UV-C irradiation.

Sample	Photocurrent at 0.5 V ($\mu A/cm^2$)	Photocurrent at 1.5 V ($\mu A/cm^2$)
Ti_1	123.3	117.2
Ti_2	153.6	117.4
Ti_3	230.3	238.6
Ti_4	228.4	218.1
Ti_5	0.2	-
Ti_6	4.0	-
TiW_1	54.7	95.8
TiW_2	13.4	33.9
TiW_3	14.6	43.7
TiW_4	94.6	118.9
TiW_5	79.3	116.4
TiW_6	135.5	141.5

As for the pure TiO_2 films, in agreement the literature [24], samples oxidized at intermediate voltages (140 and 160 V) showed the highest photocurrent, 238.6 $\mu A/cm^2$ at 1.5 V and 228.4 $\mu A/cm^2$

at 0.5 V, respectively. Oppositely, TiO_2-WO_3 films best performed at 200 V (141.5 μA/cm^2 at 1.5 V) and showed lower photocurrent values at lower cell voltages. Photocurrent values of TiO_2 and TiO_2-WO_3 films obtained at the different cell voltages are reported in table 4. Photocurrent values are considered both at 0.5 and 1.5 V because a well-defined plateau is not always present.

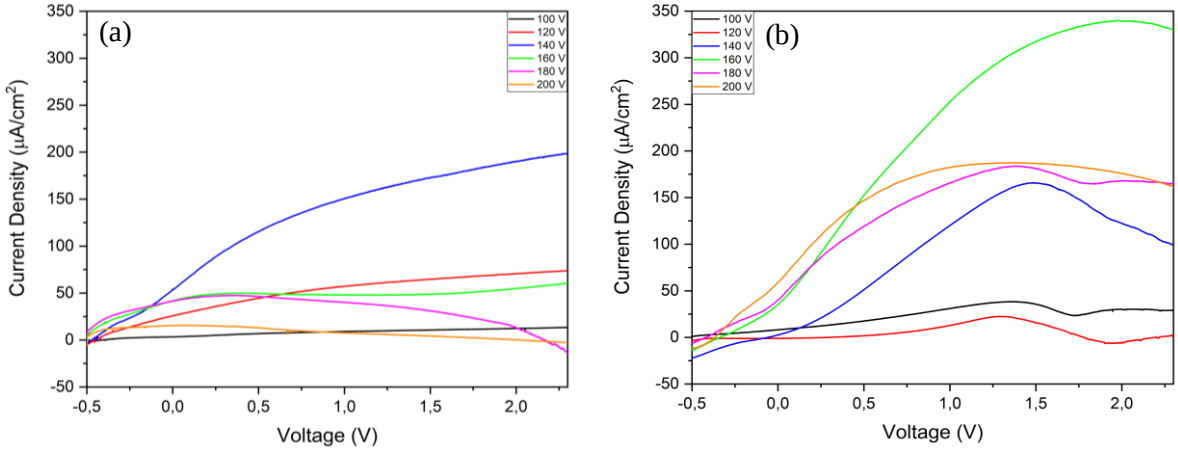

Figure 5. Photocurrent density of TiO_2 (a) and Ti-W oxide (b) samples under UV-VIS irradiation.

Table 5. Photocurrent values of TiO_2 and Ti-W oxide samples during LSV at 0.5 and 1.5 V under UV-VIS irradiation.

Sample	Photocurrent at 0.5 V (μA/cm^2)	Photocurrent at 1.5 V (μA/cm^2)
Ti_1	6.8	10.9
Ti_2	44.2	64.5
Ti_3	115.3	172.8
Ti_4	49.3	48.7
Ti_5	46.5	30.8
Ti_6	12.9	4.2
TiW_1	17.9	35.4
TiW_2	1.8	15.9
TiW_3	50.8	165.8
TiW_4	152.6	316.9
TiW_5	118.9	181.6
TiW_6	146.7	186.5

Photocurrent measurement under UV-VIS irradiation were also carried out for both TiO_2 and TiO_2-WO_3 films (figure 5). The most photoactive TiO_2 sample was obtained at 140 V, reaching 172.8 μA/cm^2 at 1.5 V. The highest photocurrent of TiO_2-WO_3 films was obtained at 160 V, with a value of 316.9 μA/cm^2 at 1.5 V. On average, TiO_2-WO_3 films outperformed pure TiO_2. This might be attributed to both the lower energy band-gap of the WO_3 phase and to the formation of favorable semiconductor heterojunctions [14]. Photocurrent values of TiO_2 and TiO_2-WO_3 films measured at 0.5 and 1.5 V are reported in table 5.

4. Conclusions

Photoactive mixed TiO_2-WO_3 films were synthetized by PEO of Ti-W surface alloys obtained by PVD-LEHCEB. The oxide films were crystalline in structure. TiO_2 consisted in a mixture of anatase and rutile phases at 100-120 V, and in almost pure rutile at higher voltages. The monoclinic crystal phase of WO_3 was also detected in all the synthetized sample. SEM surface micrographs showed a porous morphology characterized by coarser and inhomogeneous surface features with respect to pure TiO_2 films. According to EDS spectra, the average W content varied from 3.2 to 0.3 at.%. Photoelectrochemical characterization under VIS irradiation revealed that on average TiO_2-WO_3 films outperform pure TiO_2 films, demonstrating that the presence of the WO_3 phase red-shifted the light adsorption of the photoactive films compared to pure TiO_2.

References

[1] Kolli R P and Devaraj A 2018 *Metals* **8** 1–41
[2] Dobromyslov A V and Elkin V A 2001 *Scripta Mater.* **44** 905–10
[3] Callisti M, Tichelaar F D and Polcar T 2018 *J. Alloy. Compd.* **749** 1000–8
[4] Oparowski J M, Sisson R D and Biederman R R 1987 *Thin Solid Films* **153** 313–28
[5] Ozur G E 2012 *25th International Symposium on Discharges and Electrical Insulation in Vacuum* (Tomsk: IEEE) pp 580–3
[6] Zhang X D, Hao S Z, Li X N, Dong C and Grosdidier T 2011 *Appl. Surf. Sci.* **257** 5899–902
[7] Rotshtein V P, Proskurovsky D I, Ozur G E, Ivanov Y F and Markov A B 2004 *Surf. Coat. Tech.* **180**–**181** 377–81
[8] Fujishima A, Zhang X and Tryk D A 2008 *Surf. Sci. Rep.* **63** 515–82
[9] Ochiai T and Fujishima A 2012 *J. Photoch. Photobio.* C **13** 247–62
[10] Pancielejko A, Rzepnikowska M, Zaleska-Medynska A, Łuczak J and Mazierski P 2020 *Materials* **13** 3506
[11] Chiarello G L, Bernareggi M, Pedroni M, Magni M, Pietralunga S M, Tagliaferri A, Vassallo E and Selli E 2017 *J. Mater. Chem.* **5** 12977–89
[12] Siol S, Ott N, Beall C, Stiefel M, Unutulmazsoy Y, Döbeli M, Tilley S D, Schmutz P, Jeurgens L P H and Cancellieri C 2020 *Acta Mater.* **186** 95–104
[13] Soares L and Alves A 2018 *Mater. Lett.* **211** 339–42
[14] Dozzi M V, Marzorati S, Longhi M, Coduri M, Artiglia L and Selli E 2016 *Appl. Catal.* B – *Environ.* **186** 157–65
[15] Sliozberg K, Schäfer D, Erichsen T, Meyer R, Khare C, Ludwig A and Schuhmann W 2015 *ChemSusChem* **8** 1270–8
[16] Nah Y-C, Ghicov A, Kim D, Berger S and Schmuki P 2008 *J. Am. Chem. Soc.* **130** 16154–5
[17] Franz S, Perego D, Marchese O, Lucotti A and Bestetti M 2016 *Appl. Surf. Sci.* **385** 498–505
[18] Franz S, Arab H, Lucotti A, Castiglioni C, Vicenzo A, Morini F and Bestetti M 2020 *Catalysts* **10** 325
[19] Mirelman L K, Curran J A and Clyne T W 2012 *Surf. Coat. Tech.*. **207** 66–71
[20] Quintero D, Galvis O, Calderón J A, Castaño J G and Echeverría F 2014 *Surf. Coat. Tech.* **258** 1223–31
[21] Murgolo S, Franz S, Arab H, Bestetti M, Falletta E and Mascolo G 2019 *Water Res.* **164** 114920
[22] Collivignarelli M C, Abbà A, Miino M C, Arab H, Bestetti M and Franz S 2020 *J. Hazard. Mater.* **387** 121668
[23] Collivignarelli M C, Abbà A, Miino M C, Bertanza G, Sorlini S, Damiani S, Arab H, Bestetti M and Franz S 2021 *Environ. Sci. Pollut. R.* **28** 1–10
[24] Franz S, Arab H, Chiarello G L, Bestetti M and Selli E 2020 *Adv. Energy Mater.* **10** 2000652
[25] Bayati M R, Golestani-Fard F, Moshfegh A Z and Molaei R 2011 *Mater. Chem. Phys.* **128** 427–32
[26] He J, Luo Q, Cai Q Z, Li X W and Zhang D Q 2011 *Mater. Chem. Phys.* **129** 242–8